Inorganic Chemistry

pubs.acs.org/IC

Article

Structures and Magnetic Properties of $K_2Pd_4U_6S_{17}$, $K_2Pt_4U_6S_{17}$, $Rb_2Pt_4U_6S_{17}$, and $Cs_2Pt_4U_6S_{17}$ Synthesized Using the Boron−Chalcogen Mixture Method

Logan S. Breton, Ryan Baumbach, Hunter B. Tisdale, and Hans-Conrad zur Loye*

Cite This: *Inorg. Chem.* 2022, 61, 10502−10508

Read Online

ACCESS | Metrics & More | Article Recommendations | Supporting Information

ABSTRACT: A series of $A_2M_4U_6S_{17}$ (A = alkali metal; M = Pd, Pt) compounds, specifically $K_2Pd_4U_6S_{17}$, $K_2Pt_4U_6S_{17}$, $Rb_2Pt_4U_6S_{17}$, and $Cs_2Pt_4U_6S_{17}$, were synthesized using the combined boron−chalcogen mixture and molten flux crystal growth methods. The formation of rubidium- and cesium-containing analogues resulted from a *in situ* alkali polysulfide flux formed from alkali carbonates. The successful synthesis of single crystals of the title compounds allowed for their structural characterization by single-crystal X-ray diffraction. The structure determination revealed disorder of the alkali cations in $Rb_2Pt_4U_6S_{17}$ and $Cs_2Pt_4U_6S_{17}$, while the potassium cations in $K_2Pd_4U_6S_{17}$ and $K_2Pt_4U_6S_{17}$ were fully ordered. Magnetic measurements were performed on samples of $K_2Pt_4U_6S_{17}$, $Rb_2Pt_4U_6S_{17}$, and $Cs_2Pt_4U_6S_{17}$ that contained small amounts of paramagnetic β-US_2 and diamagnetic PtS. Antiferromagnetic order was observed at T_N = 9.1 K for $K_2Pt_4U_6S_{17}$. No long-range magnetic order was observed for $Rb_2Pt_4U_6S_{17}$ and $Cs_2Pt_4U_6S_{17}$. Uranium moments of 2.5, 2.6, and 2.6 μ_B were measured for $K_2Pt_4U_6S_{17}$, $Rb_2Pt_4U_6S_{17}$, and $Cs_2Pt_4U_6S_{17}$, respectively.

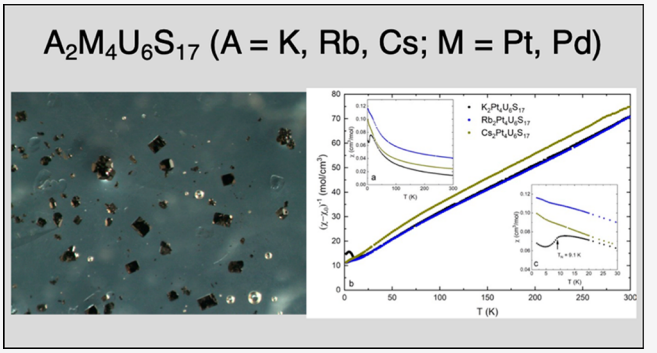

INTRODUCTION

The actinide chalcogenides are of interest for their ability to stabilize uranium's paramagnetic 4+ oxidation state, which makes it possible to study the magnetic behavior of uranium(IV). Uranium in an oxide environment is typically found in the 6+ oxidation state, which has no unpaired f electrons and is diamagnetic.[1] While uranium(IV) oxides are known, such as uranium(IV) phosphates[2,3] and silicates,[4] their synthesis is difficult.[5] On the other hand, the softer Lewis basicity of the chalcogens relative to oxygen results in most uranium chalcogenides stabilizing uranium's paramagnetic 4+ oxidation state.[6,7] The ability to stabilize uranium(IV) in complex chalcogenides has resulted in the exploration of uranium chalcogenides to study the magnetic behavior of uranium(IV).[8] In addition, such uranium chalcogenides are of interest for their strongly correlated electron states, and some of them exhibit unconventional superconductivity, such as UTe_2.

There are, however, synthetic challenges in the synthesis of actinide chalcogenides that create difficulties for performing magnetic measurements. The dominant synthetic challenge is the high oxophilicity of uranium that leads to the reaction of uranium with even trace amounts of oxygen present in the reaction mixture, resulting in uranium oxide or magnetic oxychalcogenide impurities that complicate magnetic measurements.[9−11] Our recently established boron−chalcogen mixture (BCM) method alleviates this problem by permitting the synthesis of uranium chalcogenides from oxide reagents by adding a mixture of boron and the desired chalcogen to the reagent mixture, resulting in products devoid of uranium oxide or oxychalcogenide impurities.[12] This is effected by the much larger formation energy of boron oxide, B_2O_3 [i.e., $\Delta_f G°$(vitreous B_2O_3) = −1182.5 kJ/mol], versus the boron chalcogenide, B_2S_3 [e.g., $\Delta_f G°$(vitreous B_2S_3) = −247.6 kJ/mol], favoring the formation of B_2O_3 and allowing elemental boron to act as an "oxygen sponge".[13] The formation of B_2O_3 removes oxygen from the system and leaves the chalcogen to react with the other reagents. The BCM method has been successfully employed in the solid-state synthesis of binary actinide chalcogenides and for the molten flux crystal growth of higher-order actinide chalcogenides from actinide oxide starting reagents as well as the sulfurization of ternary actinide oxides to sulfides via solid-state syntheses. The ability to use actinide oxide starting reagents to synthesize chalcogenide products greatly facilitates the ease of reaction setup, allowing

Received: April 21, 2022
Published: June 29, 2022

Table 1. Crystallographic Data for the $A_2M_4U_6S_{17}$ (A = K, Rb, Cs; M = Pd, Pt) Compounds Reported Herein

chemical formula	$K_2Pd_4U_6S_{17}$	$K_2Pt_4U_6S_{17}$	$Rb_2Pt_4U_6S_{17}$	$Cs_2Pt_4U_6S_{17}$
fw	2477.00	2831.76	2924.50	3019.38
cryst syst	tetragonal			
space group, Z	$P4/mnc$, 2			
a, Å	10.28500(14)	10.2540(2)	10.3116(2)	10.4179(2)
c, Å	12.7001(3)	12.7359(4)	12.7543(3)	12.7935(3)
V, Å^3	1343.43(5)	1339.11(7)	1356.15(6)	1388.51(6)
ρ_{calcd}, g/cm^3	6.123	7.023	7.162	7.222
radiation (λ, Å)	Mo Kα (0.71073)			
μ, mm^{-1}	40.253	58.568	61.091	58.769
T, K	300(2)	300(2)	300(2)	299(2)
cryst dimens, mm^3	0.060 × 0.040 × 0.040	0.050 × 0.050 × 0.050	0.060 × 0.060 × 0.060	0.100 × 0.050 × 0.050
2θ range, deg	2.548−36.354	2.550−30.072	2.540−30.049	2.521−30.035
reflns collected	27721	19181	19064	19377
data/param/restraints	1696/40/0	1029/40/0	1043/42/0	1067/42/0
$\Delta\rho_{max}$ (e Å^{-3})	2.341	2.387	1.406	2.898
$\Delta\rho_{min}$ (e Å^{-3})	−2.009	−1.477	−1.293	−3.839
R_{int}	0.0464	0.0512	0.0548	0.0710
goodness of fit	1.295	1.433	1.420	1.301
R_1 [$I > 2\sigma(I)$]	0.0175	0.0217	0.0170	0.0291
wR_2 (all data)	0.0387	0.0460	0.0413	0.0717

for greater access to actinide chalcogenide compositions and therefore access to the magnetic properties of uranium. Another great synthetic advantage of the BCM method is the *in situ* alkali polysulfide flux formation, which can be achieved by adding an alkali carbonate and an appropriate amount of boron and sulfur to the reaction mixture. Alkali polychalcogenide fluxes have been paramount in the formation of many chalcogenide phases but are highly moisture- and air-sensitive as well as commercially unavailable, which necessitates their synthesis "in-house" via a combination of the alkali metal and chalcogen in liquid ammonia.[14−19] The ability to create an alkali polysulfide flux *in situ* thus negates the need for premade reagents and reduces the number of highly moisture- and air-sensitive reagents.

Herein we report the synthesis, structural characterization, and magnetic properties of several $A_2M_4U_6S_{17}$ (A = alkali metal; M = Pd, Pt) compounds synthesized using the combined BCM and molten flux crystal growth methods. This work extends earlier reports by Oh concerning the synthesis of some $A_2M_4U_6Q_{17}$ (Q = chalcogen) compounds where $Rb_2Pd_4U_6S_{17}$ was reported to order antiferromagnetically at low temperature.[20,21] As detailed herein, applying the BCM method coupled with molten flux crystal growth resulted in single crystals of $K_2Pd_4U_6S_{17}$, $K_2Pt_4U_6S_{17}$, $Rb_2Pt_4U_6S_{17}$, and $Cs_2Pt_4U_6S_{17}$ whose magnetic properties were measured.

EXPERIMENTAL METHODS

Synthesis. Elemental boron (Cerac, ∼100 mesh, 99.5%), elemental sulfur (Fischer Chemical, sublimed), platinum metal (Engelhard Corp.), palladium metal (Engelhard Corp.), Cs_2CO_3 (Alfa Aesar, 99%), Rb_2CO_3 (Alfa Aesar, 99%), CsCl (VWR, ultrapure), KCl (VWR, ACS grade), and RbCl (Alfa Aesar, 99.8%) were all used as received. U_3O_8 (International Bio-Analytical Industries, Inc., 99.99%) powder was placed in a furnace set to 800 °C for 24 h and subsequently stored in a 260 °C oven. K_2S was prepared as stated in the literature and stored in a nitrogen-filled glovebag.[22] All alkali carbonates and alkali halide fluxes were kept in a 260 °C oven before use. K_2S and the alkali halide fluxes were handled inside a nitrogen-filled glovebag due to their hygroscopic nature. All grinding and mixing of reagents were performed inside the glovebag.

Caution! *Although the uranium precursor used in these syntheses contains depleted uranium, observing proper procedures for handling radioactive materials is required. All handling of radioactive materials was performed in laboratories specially designated for the study of radioactive uranium materials.*

$K_2Pd_4U_6S_{17}$ was prepared by combining 0.119 mmol of U_3O_8, 0.483 mmol of palladium, 2.377 mmol of boron, and 3.555 mmol of sulfur into an agate mortar. The agate mortar was placed in a nitrogen-filled glovebag, in which 0.907 mmol of K_2S was weighed out and added to the reagent mixture. This mixture was intimately mixed by grinding and loaded into a carbon crucible (9.525 mm o.d. × 6.35 mm i.d. × 50.8 mm length). A total of 3.353 mmol of KCl flux was loaded on top of the ground mixture inside the carbon crucible, which was subsequently placed in a fused-silica tube (12 mm o.d. × 10 mm i.d. × 203.2 mm length), which was then evacuated and flame-sealed. The silica tube was placed in a furnace set to first ramp up to 400 °C in 1 h and then slowly ramp up to 900 °C in 10 h to keep the volatile sulfur from building up enough pressure to burst the tube. After dwelling for 48 h at 900 °C, the reaction was cooled to 600 °C in 25 h and the furnace was then shut off to allow the reaction to reach room temperature. The carbon crucible was removed from the fused-silica tube, placed in a beaker of ∼60 mL of water, and sonicated to remove the flux. The water also dissolved and removed the B_2O_3 that formed during the reaction. Black block crystals of $K_2Pd_4U_6S_{17}$ were isolated via vacuum filtration along with β-US_2 and $U_{0.92}Pd_3S_4$.

$K_2Pt_4U_6S_{17}$ was prepared using the method described above by combining 0.095 mmol of U_3O_8, 0.237 mmol of platinum, 2.377 mmol of boron, 3.555 mmol of sulfur, 0.907 mmol of K_2S, and 3.353 mmol of KCl flux. Black block crystals of $K_2Pt_4U_6S_{17}$ were isolated via vacuum filtration along with β-US_2 and PtS.

$Rb_2Pt_4U_6S_{17}$ was prepared using the method described above by combining 0.095 mmol of U_3O_8, 0.237 mmol of platinum, 2.377 mmol of boron, 3.555 mmol of sulfur, 0.346 mmol of Rb_2CO_3, and 2.067 mmol of RbCl flux. Black block crystals of $Rb_2Pt_4U_6S_{17}$ were isolated via vacuum filtration along with β-US_2 and PtS.

$Cs_2Pt_4U_6S_{17}$ was prepared using the method described above by combining 0.048 mmol of U_3O_8, 0.119 of platinum, 1.184 mmol of boron, 1.781 mmol of sulfur, 0.173 mmol of Cs_2CO_3, and 1.485 mmol of CsCl flux. Black block crystals of $Cs_2Pt_4U_6S_{17}$ were isolated via vacuum filtration along with PtS.

Caution! *Exposure of boron sulfides to air or water can result in the formation of dangerous hydrogen sulfide gas. Upon heating of the reaction mixtures in fused-silica ampules, the generation of sulfur vapor and the*

https://doi.org/10.1021/acs.inorgchem.2c01363
Inorg. Chem. 2022, 61, 10502−10508

thermal decomposition of the alkali carbonates generating $CO_2(g)$ will generate an internal pressure that can cause the tube to burst violently.

Single-Crystal X-ray Diffraction (SXRD). X-ray intensity data from black block crystals of all title compounds were all collected at 300 K using a Bruker D8 QUEST diffractometer equipped with a PHOTON-II area detector and an Incoatec microfocus source (Mo Kα radiation, λ = 0.71073 Å). The raw area detector dataframes were reduced and corrected for absorption effects using the *SAINT+* and *SADABS* programs.[23,24] Final unit cell parameters were determined by least-squares refinement of large sets of reflections taken from each data set. An initial structural model was obtained with *SHELXT*.[25] Subsequent difference Fourier calculations and full-matrix least-squares refinement against F^2 were performed with *SHELXL-2018* using the *Olex2* interface.[26,27] For $Rb_2Pt_4U_6S_{17}$ and $Cs_2Pt_4U_6S_{17}$, the free refinement of the alkali-metal positions resulted in less than full occupancy as well as a significant q peak close to the assigned crystallographic position. Refining the alkali metals using a split site model reduced the R factor and flattened the residual electron density map. The crystallographic data are summarized in Table 1. Atomic coordinates for each compound are available in Tables S1−S4.

Powder X-ray Diffraction (PXRD). PXRD data were collected on ground samples of the products obtained. Data were collected on a Bruker D2 PHASER diffractometer using Cu Kα radiation over a 2θ range of 5−65° with a step size of 0.02°. A Whole Powder Pattern Fit (WPPF) was performed on the PXRD patterns obtained from the product powders of reactions targeting $K_2Pt_4U_6S_{17}$, $Rb_2Pt_4U_6S_{17}$, and $Cs_2Pt_4U_6S_{17}$ using the Rigaku *SmartLab II Studio* software.[28] WPPF analysis allowed for determination of the relative weight percent of the target phase, β-US_2, and PtS within each product powder. The PXRD patterns and WPPF are shown in Figures S1−S4 and S5−S7, respectively.

Energy-Dispersive Spectroscopy (EDS). EDS was performed on single crystals of the title compounds using a Tescan Vega-3 scanning electron microscope equipped with a Thermo EDS attachment. Scanning electron microscopy (SEM) was operated in a low-vacuum mode. Crystals were mounted on a SEM stub with carbon tape and analyzed using a 20 kV accelerating voltage and an 80 s accumulation time. The EDS spectra for the crystals are shown in Figures S8−S11. The results of EDS confirmed the presence of elements found by SXRD and are summarized in Tables S5 and S6.

Magnetic Measurements. Magnetic susceptibility measurements were carried out over the temperature range of T = 1.8−300 K in an applied magnetic field of H = 0.5 T using a Quantum Design VSM Magnetic Property Measurement System. Measurements were performed on randomly oriented polycrystalline specimens that were loaded into VSM powder holders with a diameter of 2.60 mm. The powder holders were then suspended within straws and attached to the sample transport rod for measurements. The sample masses were 19.59, 33.56, and 16.85 mg for $K_2Pt_4U_6S_{17}$, $Rb_2Pt_4U_6S_{17}$, and $Cs_2Pt_4U_6S_{17}$, respectively.

DISCUSSION

Synthesis. Single crystals of the compounds reported herein were synthesized using the combined BCM and molten flux growth methods (Figure 1). The BCM method allowed for the use of uranium oxide, U_3O_8, as the uranium source for all reactions and the *in situ* generation of alkali polysulfide fluxes from their respective alkali carbonates for the cesium- and rubidium-containing reactions, avoiding the use of highly air- and moisture-sensitive alkali polysulfide fluxes. Exploratory synthesis trials determined that the addition of both alkali polysulfide and alkali halide fluxes was necessary to obtain highly crystalline products of the target phases. Initial attempts at the synthesis of $K_2Pd_4U_6S_{17}$ performed without the addition of the potassium sulfide flux only resulted in products containing chunks of palladium metal, black rods of β-US_2, and black blocks of $U_{0.92}Pd_3S_4$, while reactions targeting $K_2Pt_4U_6S_{17}$ only yielded crystalline β-US_2 and PtS. No trace of the title compounds was observed among the reaction products. On the other hand, reactions foregoing the use of the alkali halide flux and only using the potassium sulfide flux resulted in products containing poorly crystalline products of $K_2Pt_4U_6S_{17}$, β-US_2, and KPt_2S_3 in reactions targeting $K_2Pt_4U_6S_{17}$ and poorly crystalline products of $K_2Pd_4U_6S_{17}$, β-US_2, and $U_{0.90}Pd_3S_4$ in reactions targeting $K_2Pd_4U_6S_{17}$. Reactions that utilized both the alkali halide and potassium sulfide fluxes resulted in highly crystalline products of $K_2Pt_4U_6S_{17}$, β-US_2, and PtS in reactions targeting $K_2Pt_4U_6S_{17}$ and highly crystalline products of $K_2Pd_4U_6S_{17}$, β-US_2, and $U_{0.92}Pd_3S_4$ in reactions targeting $K_2Pd_4U_6S_{17}$. These observations indicate that using both the potassium sulfide and alkali halide fluxes is the best route for the synthesis of highly crystalline products of the compounds reported herein.

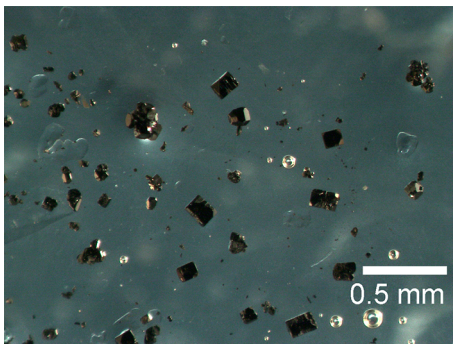

Figure 1. Image of the black block crystals of $K_2Pt_4U_6S_{17}$.

After the successful synthesis of both $K_2Pd_4U_6S_{17}$ and $K_2Pt_4U_6S_{17}$, we chose to test the BCM method's ability to create *in situ* alkali polysulfide fluxes from alkali carbonates, thus avoiding having to prepare the alkali sulfide reagents ahead of time. In reactions targeting the $Rb_2Pt_4U_6S_{17}$ and $Cs_2Pt_4U_6S_{17}$ analogues, the synthetic procedures were kept the same as those used for $K_2Pd_4U_6S_{17}$ and $K_2Pt_4U_6S_{17}$, except for the replacement of an alkali polysulfide flux with Rb_2CO_3 or Cs_2CO_3. The resulting products obtained were highly crystalline single crystals of $Rb_2Pt_4U_6S_{17}$ and $Cs_2Pt_4U_6S_{17}$, supporting the successful *in situ* formation of the alkali polysulfide flux by the BCM method. Attempts at creating phase-pure powders for all target phases were unfortunately unsuccessful as crystalline β-US_2 and MS (M = Pt, Pd) persisted in the reaction products even after variation of the relative reactant ratios and reaction temperatures. In reactions targeting the platinum-containing phases, the reagent ratios were extensively varied in attempts to reduce the β-US_2 and PtS impurities, and while feasible, further reduction of the uranium and platinum reagent ratios also prevented the title compounds from forming. The same attempts were carried out to obtain pure $K_2Pd_4U_6S_{17}$; however, it was not possible to avoid the formation of some $U_{0.92}Pd_3S_4$ and β-US_2 impurities.

Structure Description. The compounds reported herein join the family of $A_2M_4U_6Q_{17}$ compounds that crystallize in the tetragonal crystal system adopting the space group $P4/mnc$. The structure is comprised of two crystallographically unique uranium sites, U1 and U2, and one unique M (M = Pt, Pd) site. Figure 2 shows the local coordination environments for metal cations in each structure.

The structure consists of four unique layers, designated as A, A′, B, and B′, oriented in the *ab* plane, as shown in Figure 3. Layer A is composed of $U1_4S_{17}$ tetramers that are connected

https://doi.org/10.1021/acs.inorgchem.2c01363
Inorg. Chem. 2022, 61, 10502−10508

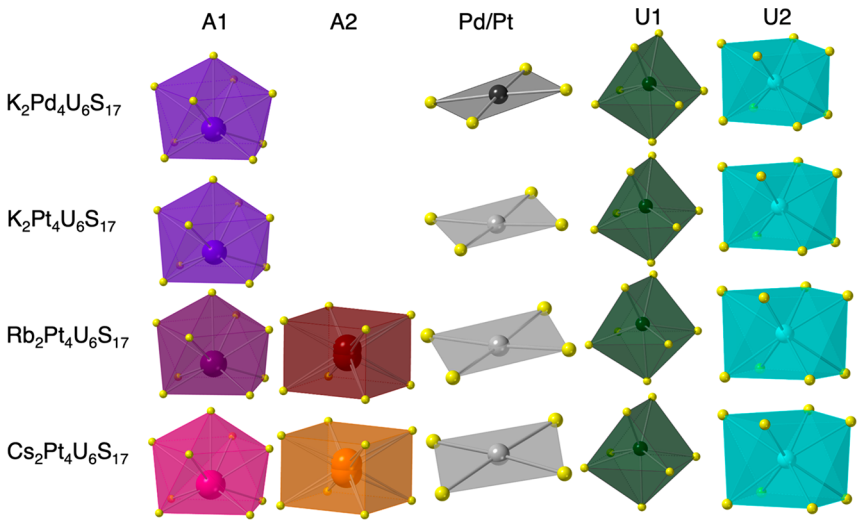

Figure 2. Representations of local coordination polyhedra for the metal atoms within each $A_2M_4U_6S_{17}$ compound reported herein. $K_2Pd_4U_6S_{17}$ and $K_2Pt_4U_6S_{17}$ have only one alkali metal site, while $Rb_2Pt_4U_6S_{17}$ and $Cs_2Pt_4U_6S_{17}$ have a split site for the alkali metal and, hence, two coordination polyhedra of the alkali metals are shown for them.

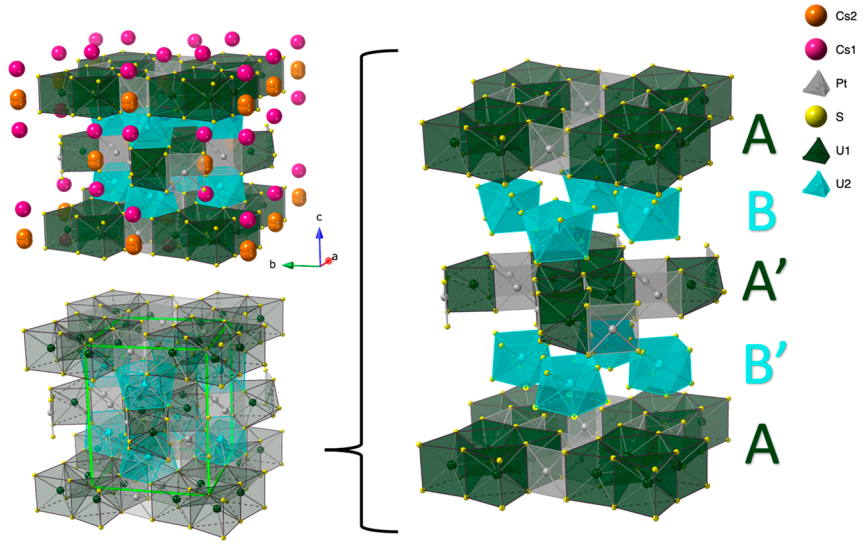

Figure 3. (top left) Image of the representative structure of $Cs_2Pt_4U_6S_{17}$ and (bottom left) image showing the arrangement of the atoms within the unit cell and (right) schematic of the separate layers within the structure and how they stack.

via MS_4 (M = Pd, Pt) square-planar units. The tetramers are created by four 7-coordinate US_7 monocapped trigonal prisms that are connected by sharing the S3 atom occupying the capping position of the monocapped trigonal prism and S1 atoms making up two sides of the trigonal prism. This results in each monocapped trigonal prism sharing two triangular faces with two adjacent polyhedra. These $U1_4S_{17}$ tetramers connect to each other within the layer through edge-sharing MS_4 square-planar units. The MS_4 units use two S1 atoms of one tetramer and two S2 atoms of another. Layer A′ is identical with layer A in composition but is rotated ∼37° and translated by $^1/_2a$ and $^1/_2b$. Layers B and B′ are mirror images of one another and are composed of isolated $U2S_8$ square antiprisms that link layers A and A′ through edge sharing with two MS_4 square-planar units in the layers above and two below them. Layers B and B′ alternate with the A and A′ layers, resulting in an overall stacking sequence of ABA′B′. To visualize the stacking of these layers, Figure 3 illustrates the position of each layer within the unit cell. The cesium cations fill the void spaces within $U1_4S_{17}$ tetramers and $U2S_8$ square antiprisms within the layers of the structure.

In $K_2Pd_4U_6S_{17}$ and $K_2Pt_4U_6S_{17}$, crystallographically ordered potassium cations fill the spaces within the B and B′ layers. Structure solutions of $Rb_2Pt_4U_6S_{17}$ and $Cs_2Pt_4U_6S_{17}$, on the other hand, refined best when modeling the A cation positions split over two sites (A1 and A2; Figure 4). A similar split position for the alkali-metal cations was previously reported for the structures of $Rb_2Pt_4U_6Se_{17}$ and $Cs_2Pt_4U_6Se_{17}$.[21]

In $K_2Pd_4U_6S_{17}$, the Pd−S distances range from 2.3403(8) to 2.3662(8) Å and the U−S distances range from 2.6796(8) to 2.8717(8) Å. In $K_2Pt_4U_6S_{17}$, $Rb_2Pt_4U_6S_{17}$, and $Cs_2Pt_4U_6S_{17}$, the Pt−S distances range from 2.3413(13) to 2.3711(15) Å, and the U−S distances range from 2.6893(13) to 2.9285(18) Å. Uranium is in its 4+ oxidation state, which is supported by charge balance, the lack of S−S bonds, and bond-valence-sum calculations that indicate average uranium oxidation states of 4.04, 3.97, 3.96, and 3.90 for $K_2Pd_4U_6S_{17}$, $K_2Pt_4U_6S_{17}$, $Rb_2Pt_4U_6S_{17}$, and $Cs_2Pt_4U_6S_{17}$, respectively.

https://doi.org/10.1021/acs.inorgchem.2c01363
Inorg. Chem. 2022, 61, 10502−10508

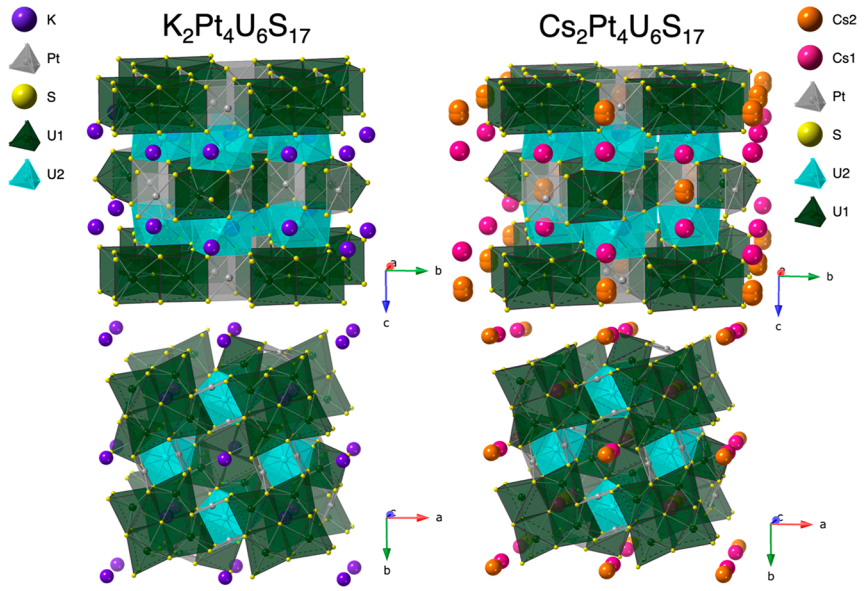

Figure 4. (left) Image showing an example of ordered potassium cations (purple) observed in $K_2Pt_4U_6S_{17}$ and $K_2Pd_4U_6S_{17}$. (right) Example of alkali cations split over two positions. In this case, the Cs cation is split into Cs1 (pink) and Cs2 (orange), as observed in $Rb_2Pt_4U_6S_{17}$ and $Cs_2Pt_4U_6S_{17}$.

Magnetic Susceptibility Measurements. Magnetic measurements were performed on ground samples of $K_2Pt_4U_6S_{17}$, $Rb_2Pt_4U_6S_{17}$, and $Cs_2Pt_4U_6S_{17}$ containing small amounts of the β-US_2 and PtS impurities. PtS is diamagnetic and β-US_2 is paramagnetic over the 2−300 K range.[29,30] Therefore, any observed magnetic transition would be due to $K_2Pt_4U_6S_{17}$, $Rb_2Pt_4U_6S_{17}$, or $Cs_2Pt_4U_6S_{17}$. WPPF was performed using the Rigaku *SmartLab II Studio* software to obtain the relative weight percent of the impurity phases (Table 2) to correct the sample mass for the impurity upon calculation of the molar magnetic susceptibility. No magnetic measurements were performed for $K_2Pd_4U_6S_{17}$ because of the inability to separate the black blocks of $U_{0.92}Pd_3S_4$, which orders magnetically, from the black blocks of $K_2Pd_4U_6S_{17}$.[31]

Table 2. Results of WPPF Showing the Relative Weight Percent of Each Phase in the Product Powders

sample	target product (%)	US_2 (%)	PtS (%)
$K_2Pt_4U_6S_{17}$	96.61(19)	2.25(17)	1.14(10)
$Rb_2Pt_4U_6S_{17}$	92.8(3)	4.2(3)	2.98(17)
$Cs_2Pt_4U_6S_{17}$	96.82(9)	N/A	3.18(9)

Figure 5 contains a plot of the magnetic susceptibility data for compounds $A_2Pt_4U_6S_{17}$ (A = K, Rb, Cs). Paramagnetic behavior is observed at elevated temperatures, similar to what was reported for the isostructural analogue $Rb_2Pd_4U_6S_{17}$.[21] The 150−300 K data were fitted using a modified Curie−Weiss expression $\chi = \chi_0 + C/(T - \theta)$, where χ_0 is a temperature-independent term, C is the Curie constant, and θ is the Curie−Weiss temperature. The results of the fits are listed in Table 3, where the negative θ values indicate the presence of antiferromagnetic correlations between the uranium ions. The origin of the χ_0 term remains to be identified, but we point out that magnetic data for even single-crystal specimens of $Rb_2Pd_4U_6S_{17}$ result in similar χ_0 terms whose absolute value is reduced from what is seen here. It is reasonable to suggest that, for these samples, the impurity phases may contribute to this term. The effective magnetic moment per uranium was determined and found to range from 2.5 to 2.6 μ_B for the three phases. These values are reduced from the expected moment of tetravalent uranium of 3.58 μ_B calculated using full Russell−Saunders coupling for a $^3H_4$ ground state. The published moments of uranium(IV) range

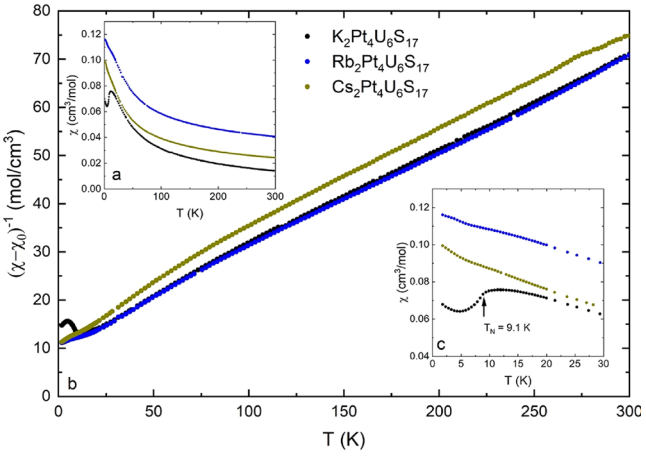

Figure 5. (a) Temperature-dependent magnetic susceptibility $\chi(T)$ collected in an applied magnetic field H = 5000 Oe for compounds $A_2Pt_4U_6S_{17}$ (A = K, Rb, Cs). (b) $(\chi - \chi_0)^{-1}$ versus T, where the linear behavior that is seen for T > 150 K was fitted using a modified Curie−Weiss function as described in the text. (c) Low-temperature zoom of $\chi(T)$ emphasizing the antiferromagnetic ordering at T_N = 9.1 K for $K_2Pt_4U_6S_{17}$ and the absence of bulk ordering for $Rb_2Pt_4U_6S_{17}$ and $Cs_2Pt_4U_6S_{17}$. A plot showing the overlap of the zero-field-cooled and field-cooled data can be seen in Figure S12.

Table 3. Summary of the Magnetic Properties of $A_2Pt_4U_6S_{17}$ (A = K, Rb, Cs)

	χ_0 (cm^3/mol)	θ (K)	C (cm^3·K/mol)	μ_{eff}/U	T_N (K)
$K_2Pt_4U_6S_{17}$	0	−62	5.1	2.6	9.1
$Rb_2Pt_4U_6S_{17}$	0.027	−59	5.1	2.6	
$Cs_2Pt_4U_6S_{17}$	0.011	−71	4.7	2.5	

https://doi.org/10.1021/acs.inorgchem.2c01363
Inorg. Chem. 2022, 61, 10502−10508

from 1.36 to 3.79.[8] A reduced moment was also reported for $Rb_2Pd_4U_6S_{17}$, where it was attributed to crystal electric field effects. Because uranium magnetism is known to deviate from Hund's rule expectations due to (i) strong spin−orbit coupling and (ii) the tendency of the uranium(IV) f electrons to take on a singlet ground state at low temperatures, moments lower than the expected 3.58 μ_B are common. Further work is needed to clarify this question, but broadly speaking, this behavior is consistent with what is seen for many other uranium-based materials in which the gradual transition from a triplet to a singlet ground state for the two f electrons impacts the measured magnetic moment.[32]

An antiferromagnetic transition is observed at T_N = 9.1 K for $K_2Pt_4U_6S_{17}$, similar to what is seen for $Rb_2Pd_4U_6S_{17}$. In contrast, both $Rb_2Pt_4U_6S_{17}$ and $Cs_2Pt_4U_6S_{17}$ show weak inflections in their χ versus T plots over a similar temperature range. Reports in the literature indicate that the presence or absence of long-range magnetic order in uranium(IV) compounds in which uranium is the only magnetically active ion is a function of the U−U separation within the crystal structure, which effects the magnetic coupling ability of the uranium ions.[20,21] In the compounds reported herein, an increase in the U−U distances occurs with an increase in the size of the alkali cation (K < Rb < Cs), as illustrated in Figure 6, which is expected to reduce the ability of the uranium ions

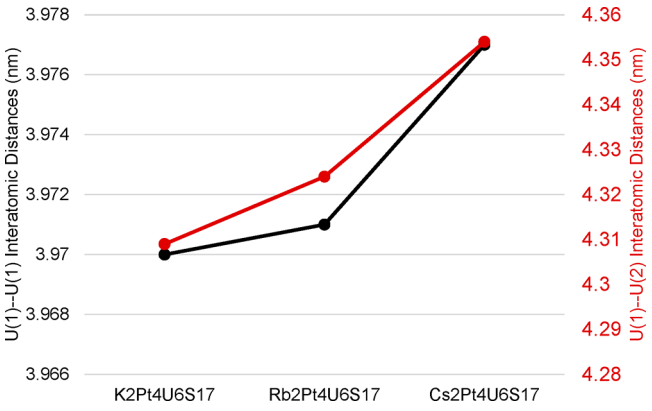

Figure 6. Plot of the (black) U1−U1 and (red) U1−U2 interatomic distances. The U2−U2 distances were excluded because they are too large (>7 Å) to have magnetic coupling between them. There is an increase in the U−U distances with an increase in the alkali cation incorporated into the $A_2Pt_4U_6S_{17}$ (A = K, Rb, Cs) structure.

to couple magnetically. It is therefore not surprising that only the potassium-containing material, $K_2Pt_4U_6S_{17}$, exhibits long-range magnetic order.

CONCLUSIONS

A series of $A_2M_4U_6S_{17}$ (A = alkali metal; M = Pd, Pt) compounds, specifically $K_2Pd_4U_6S_{17}$, $K_2Pt_4U_6S_{17}$, $Rb_2Pt_4U_6S_{17}$, and $Cs_2Pt_4U_6S_{17}$, were synthesized using the combined BCM and molten flux crystal growth methods, with the rubidium- and cesium-containing analogues taking advantage of the *in situ* alkali polysulfide flux formation from alkali carbonates. The successful synthesis of single crystals of the title compounds allowed for their structure determination. Magnetic measurements were performed on samples of $K_2Pt_4U_6S_{17}$, $Rb_2Pt_4U_6S_{17}$, and $Cs_2Pt_4U_6S_{17}$, and antiferromagnetic order is observed at T_N = 9.1 K for $K_2Pt_4U_6S_{17}$. In contrast, while both $Rb_2Pt_4U_6S_{17}$ and $Cs_2Pt_4U_6S_{17}$ show weak inflections in their χ versus T data over similar temperature ranges, they do not exhibit a magnetic transition. The absence of long-range magnetic order in the rubidium and cesium analogues is attributed to the increased U−U interatomic distances as a function of the increased size of the alkali cations. Uranium moments of 2.5, 2.6, and 2.6 μ_B were calculated for $K_2Pt_4U_6S_{17}$, $Rb_2Pt_4U_6S_{17}$, and $Cs_2Pt_4U_6S_{17}$, respectively. The BCM method enables ease of access to actinide chalcogenide phases, and its use is expected to result in further successful syntheses of actinide chalcogenide and other chalcogenide phases.

ASSOCIATED CONTENT

Supporting Information

The Supporting Information is available free of charge at https://pubs.acs.org/doi/10.1021/acs.inorgchem.2c01363.

Atomic coordinates, PXRD patterns, WPPF analyses, EDS spectra, elemental compositions, and zero-field-cooled and field-cooled magnetic plot (PDF)

Accession Codes

CCDC 2166395−2166398 contain the supplementary crystallographic data for this paper. These data can be obtained free of charge via www.ccdc.cam.ac.uk/data_request/cif, or by emailing data_request@ccdc.cam.ac.uk, or by contacting The Cambridge Crystallographic Data Centre, 12 Union Road, Cambridge CB2 1EZ, UK; fax: +44 1223 336033.

AUTHOR INFORMATION

Corresponding Author

Hans-Conrad zur Loye − *Department of Chemistry and Biochemistry, University of South Carolina, Columbia, South Carolina 29208, United States*; Email: zurloye@mailbox.sc.edu

Authors

Logan S. Breton − *Department of Chemistry and Biochemistry, University of South Carolina, Columbia, South Carolina 29208, United States*

Ryan Baumbach − *Department of Physics and National High Magnetic Field Laboratory, Florida State University, Tallahassee, Florida 32306, United States*

Hunter B. Tisdale − *Department of Chemistry and Biochemistry, University of South Carolina, Columbia, South Carolina 29208, United States*

Complete contact information is available at: https://pubs.acs.org/10.1021/acs.inorgchem.2c01363

Notes

The authors declare no competing financial interest.

ACKNOWLEDGMENTS

Research supported by the U.S. Department of Energy, Office of Basic Energy Sciences, Division of Materials Sciences and Engineering, under Award DE-SC0018739. Synthesis and structural characterization performed at University of South Carolina. Magnetic measurements collected at the National High Magnetic Field Laboratory, which is supported by the National Science Foundation Cooperative Agreement DMR-1644779 and the State of Florida.

REFERENCES

(1) Serezhkin, V. N. Some features of Stereochemistry of U(VI). In *Structural Chemistry of Inorganic Actinide Compounds*; Krivovichev, S., Burns, P., Tananaev, I., Eds.; Elsevier, 2006; pp 31−65.

(2) Bamberger, C. E.; Haire, R. G.; Begun, G. M.; Hellwege, H. E. The synthesis and characterization of crystalline phosphates of thorium, uranium and neptunium. *J. less-common met.* **1984**, *102*, 179−186.

(3) Usman, M.; Morrison, G.; Klepov, V. V.; Smith, M. D.; zur Loye, H.-C. Flux crystal growth, structure, magnetic and optical properties of a family of alkali uranium(IV) phosphates. *J. Solid State Chem.* **2019**, *270*, 19−26.

(4) Morrison, G.; Ramanantoanina, H.; Urland, W.; Smith, M. D.; zur Loye, H.-C. Flux Synthesis, Structure, Properties, and Theoretical Magnetic Study of Uranium(IV)-Containing $A_2USi_6O_{15}$ (A = K, Rb) with an Intriguing Green-to-Purple, Crystal-to-Crystal Structural Transition in the K Analogue. *Inorg. Chem.* **2015**, *54*, 5504−5511.

(5) Juillerat, C. A.; Klepov, V. V.; Morrison, G.; Pace, K. A.; zur Loye, H.-C. Flux crystal growth: a versatile technique to reveal the crystal chemistry of complex uranium oxides. *Dalton Trans.* **2019**, *48*, 3162−3181.

(6) Bugaris, D. E.; Ibers, J. A. Syntheses and characterization of some solid-state actinide (Th, U, Np) compounds. *Dalton Trans* **2010**, *39*, 5949−5964.

(7) Narducci, A. A.; Ibers, J. A. Ternary and Quaternary Uranium and Thorium Chalcogenides. *Chem. Mater.* **1998**, *10*, 2811−2823.

(8) Kindra, D. R.; Evans, W. J. Magnetic susceptibility of uranium complexes. *Chem. Rev.* **2014**, *114*, 8865−8882.

(9) Mesbah, A.; Prakash, J.; Beard, J. C.; Pozzi, E. A.; Tarasenko, M. S.; Lebègue, S.; Malliakas, C. D.; Van Duyne, R. P.; Ibers, J. A. Positional flexibility: syntheses and characterization of six uranium chalcogenides related to the 2H hexagonal perovskite family. *Inorg. Chem.* **2015**, *54*, 2851−2857.

(10) Mesbah, A.; Ibers, J. A. Syntheses and crystal structures of three barium uranium sulfides. *J. Solid State Chem.* **2013**, *199*, 253−257.

(11) Ward, M. D.; Ibers, J. A. The Synthesis and Crystal Structure of $U_7O_2Se_{12}$. *Z. fur Anorg. Allg. Chem.* **2014**, *640*, 1585−1588.

(12) Breton, L. S.; Klepov, V. V.; zur Loye, H.-C. Facile Oxide to Chalcogenide Conversion for Actinides Using the Boron-Chalcogen Mixture Method. *J. Am. Chem. Soc.* **2020**, *142*, 14365−14373.

(13) Wu, L. M.; Seo, D. K. New solid-gas metathetical synthesis of binary metal polysulfides and sulfides at intermediate temperatures: utilization of boron sulfides. *J. Am. Chem. Soc.* **2004**, *126*, 4676−4681.

(14) Bugaris, D. E.; Ibers, J. A. $RbAuUSe_3$, $CsAuUSe_3$, $RbAuUTe_3$, and $CsAuUTe_3$: Syntheses and structure; magnetic properties of RbAuUSe3. *J. Solid State Chem.* **2009**, *182*, 2587−2590.

(15) Cody, J. A.; Ibers, J. A. Uranium Tellurides: New One- and Two-Dimensional Compounds $CsUTe_6$, $CsTiUTe_5$, $Cs_8Hf_5UTe_{30.6}$, and $CsCuUTe_3$. *Inorg. Chem.* **1995**, *34*, 3165−3172.

(16) Laing, C. C.; Shen, J.; Quintero, M. A.; Weiss, B. E.; Xia, Y.; Li, Z.; He, J.; Wolverton, C.; Kanatzidis, M. G. Homologous Alkali Metal Copper Rare-Earth Chalcogenides $A_2Cu_{2n}Ln_4Q_{7+n}$ (n = 1, 2, 3). *Chem. Mater.* **2022**, *34*, 3409.

(17) Wells, D. M.; Jin, G. B.; Skanthakumar, S.; Haire, R. G.; Soderholm, L.; Ibers, J. A. Quaternary neptunium compounds: syntheses and characterization of $KCuNpS_3$, $RbCuNpS_3$, $CsCuNpS_3$, $KAgNpS_3$, and $CsAgNpS_3$. *Inorg. Chem.* **2009**, *48*, 11513−11517.

(18) Yao, J.; Wells, D. M.; Chan, G. H.; Zeng, H. Y.; Ellis, D. E.; Van Duyne, R. P.; Ibers, J. A. Syntheses, structures, physical properties, and electronic properties of some $AMUQ_3$ compounds (A = alkali metal, M = Cu or Ag, Q = S or Se). *Inorg. Chem.* **2008**, *47*, 6873−6879.

(19) Kanatzidis, M. G. Discovery-Synthesis, Design, and Prediction of Chalcogenide Phases. *Inorg. Chem.* **2017**, *56*, 3158−3173.

(20) Oh, G. N.; Choi, E. S.; Ibers, J. A. Syntheses and characterization of nine quaternary uranium chalcogenides among the compounds $A_2M_3UQ_6$ (A = K, Rb, Cs; M = Pd, Pt; Q = S, Se). *Inorg. Chem.* **2012**, *51*, 4224−4230.

(21) Oh, G. N.; Choi, E. S.; Lu, J.; Koscielski, L. A.; Ward, M. D.; Ellis, D. E.; Ibers, J. A. Syntheses and characterization of six quaternary uranium chalcogenides $A_2M_4U_6Q_{17}$ (A = Rb or Cs; M = Pd or Pt; Q = S or Se). *Inorg. Chem.* **2012**, *51*, 8873−8881.

(22) Sutorik, A. C.; Patschke, R.; Schindler, J.; Kannewurf, C. R.; Kanatzidis, M. G. Valence fluctuations and metallic behavior in $K_6Cu_{12}U_2S_{15}$, a new quaternary sulfide with a unique three-dimensional cubic framework. *Chem. Eur. J.* **2000**, *6*, 1601−1607.

(23) *APEX3*, version 2019.1-0, and *SAINT+*, version 8.40A; Bruker Nano, Inc., 2019.

(24) Krause, L.; Herbst-Irmer, R.; Sheldrick, G. M.; Stalke, D. SADABS-2016/2. *J. Appl. Crystallogr.* **2015**, *48*, 3−10.

(25) Sheldrick, G. M. SHELXT - integrated space-group and crystal-structure determination. *Acta Crystallogr. A* **2015**, *71*, 3−8.

(26) Sheldrick, G. M. A short history of SHELX. *Acta Crystallogr. A* **2008**, *64*, 112−122.

(27) Dolomanov, O. V.; Bourhis, L. J.; Gildea, R. J.; Howard, J. A. K.; Puschmann, H. OLEX2: a complete structure solution, refinement and analysis program. *J. Appl. Crystallogr.* **2009**, *42*, 339−341.

(28) *SmartLab Studio II*, version 4.5.286.0; Rigaku, 2021.

(29) Rozhdestvina, V. I.; Udovenko, A. A.; Rubanov, S. V.; Mudrovskaya, N. V. Structural investigation of cooperite (PtS) crystals. *Crystallography Reports* **2016**, *61*, 193−202.

(30) Suski, W.; Gibiński, T.; Wojakowski, A.; Czopnik, A. The crystal structure and magnetic and electrical properties of β-US_2. *Physica Status Solidi (a)* **1972**, *9*, 653−658.

(31) Fujino, T.; Sato, N.; Yamada, K.; Masuda, H.; Wakeshima, M. Crystal structure and magnetic susceptibility of uranium palladium sulfide bronze, $U_xPd_3S_4$. *J. Alloys Compd.* **1998**, *271*−*273*, 452−455.

(32) Yeon, J.; Smith, M. D.; Tapp, J.; Möller, A.; zur Loye, H. C. Application of a mild hydrothermal approach containing an in situ reduction step to the growth of single crystals of the quaternary U(IV)-containing fluorides $Na_4MU_6F_{30}$ (M = Mn2+, Co2+, Ni2+, Cu2+, and Zn2+) crystal growth, structures, and magnetic properties. *J. Am. Chem. Soc.* **2014**, *136*, 3955−3963.

https://doi.org/10.1021/acs.inorgchem.2c01363
Inorg. Chem. 2022, 61, 10502−10508